Wear 303 (2013) 78–82

Contents lists available at SciVerse ScienceDirect

Wear

journal homepage: www.elsevier.com/locate/wear

Nanoscratch in highly oriented $FeSe_{0.5}Te_{0.5}$ superconductor

Alcione Roberto Jurelo [a,*], Francisco Carlos Serbena [a], Gelson Biscaia de Souza [a], Carlos Eugênio Foerster [a], Nilson Biagini Sabino [a], Simone Aparecida da Silva [a], Cristiano Santos Lopes [a], Jorge Luiz Pimentel Júnior [b]

[a] Departamento de Física, Universidade Estadual de Ponta Grossa, Av. Gen. Carlos Cavalcanti 4748, 84.030-000 Ponta Grossa, Paraná, Brazil
[b] Instituto de Física, Universidade Federal do Rio Grande do Sul, Caixa Postal 15.051, 91.501-970 Porto Alegre, Rio Grande do Sul, Brazil

ARTICLE INFO

Article history:
Received 26 April 2012
Received in revised form
20 November 2012
Accepted 24 January 2013
Available online 20 February 2013

Keywords:
FeSe(Te)
Iron-based superconductor
Chalcogenide superconductors
Instrumented indentation
Nanoscratch

ABSTRACT

Tribological properties of highly oriented lamellar $FeSe_{0.5}Te_{0.5}$ superconductor samples were investigated. Nanoscratch morphologies and profiles were characterized by instrumented indentation, SEM and AFM. Anisotropies of the scratch morphologies of the *ab*- and *a*(*b*)*c*-planes were observed. Plowing seems to be the main mechanism of scratch deformation in the *ab*-plane, with plenty of material pile-up around the scars. Distinctively, microcracking is the dominant deformation process in the *a*(*b*)*c*-plane. Also, the scratch resistance of the *a*(*b*)*c*-plane is higher than the *ab*-plane, which presented scratch hardness values of 1.5 GPa and 0.6 GPa, respectively. Cracks were observed in the *a*(*b*)*c*-plane parallel to the *c*-axis. These observations are consistent with the deformation mechanism of cracks running perpendicular to the *c*-axis in the same *a*(*b*)*c*-plane, produced by indentations.

Published by Elsevier B.V.

1. Introduction

The discovery of superconductivity in the iron-based superconductors has attracted worldwide attention in the past three years [1,2]. Up to now, a variety of iron-based superconductors such as 1111 (REFeAs(O,F)) [1], 122 ($(Ba,K)Fe_2As_2$) [3], 11 (Fe(Se,Te)) [4] and 111 (LiFeAs) [5], were discovered. The Fe chalcogenide superconductors $FeSe_xTe_{1-x}$ has been one of the most studied among these systems. FeSe(Te) family has an extremely simple structure with only FeSe(Te) layers stacked along the *c*-axis without any intercalating cations [4]. FeSe(Te) crystallizes in the simple binary layer anti-PbO structure (*P4/nmm*). $FeSe_x$ is superconducting at $T_C \cong 8.5$ K [4] but it can be raised to 15 K [6] by partial replacement of Se by Te. By applying high pressure, T_C can reach up to 27 K under 4.5 GPa [7].

Pimentel et al. reported the mechanical properties of polycrystalline $FeSe_x$ superconductor [8,9]. The authors evaluated that the elastic modulus is around 42 GPa and that the hardness is around 1.3 GPa. The ratio between the elastic modulus and hardness for this material is situated between those of metals and brittle materials. Also, hardness and elastic modulus on the *ab*- and *a*(*b*)*c*-plane of highly oriented $FeSe_{0.5}Te_{0.5}$ melt-textured were investigated by instrumented indentation by the same research group [10]. No significant differences in hardness and elastic modulus were observed between *ab*- and *a*(*b*)*c*-planes. Hardness profiles indicated values in the range 0.6–0.8 GPa at deep tip penetration depths, while the elastic modulus showed values between 20 and 25 GPa. Cracking was occasionally observed in the *ab*-plane and at low loads.

The aim of this work was to evaluate the tribological behavior of highly oriented $FeSe_{0.5}Te_{0.5}$ superconductor. The oriented samples along the *c*-axis were prepared by a self-flux method. Scanning electron microscopy showed that the samples are characterized by a stacking of plate-like crystals that resulted into a lamellar microstructure. The tribological behavior was studied by using an instrumented indentation device adapted to the scratch mode. It was observed that the scratch is shallower than that in the *ab*-plane indicating the *a*(*b*)*c*-plane presents higher resistance to scratch. And also, inside the scratch, it is possible to observe several cracks running parallel to the *c*-axis all the length of the scratch.

2. Experimental details

$FeSe_{0.5}Te_{0.5}$ samples oriented along the *c*-axis were prepared by a self-flux method. More details about the growth method and characterization by other techniques can be found in Ref. [10]. In the *ab*-plane, the tribo-mechanical tests were performed directly on the surface due to the highly oriented surfaces along the c-axis. On the *a*(*b*)*c*-plane, samples were mounted in a low-cure temperature

* Corresponding author. Tel.: +55 42 3220 3044; fax: +55 42 3220 3042.
E-mail address: arjurelo@uepg.br (A.R. Jurelo).

0043-1648/$ - see front matter Published by Elsevier B.V.
http://dx.doi.org/10.1016/j.wear.2013.01.096

resin and then polished. Finishing was achieved with a 1 μm diamond paste.

The nanoscratch tests were performed in the *ab*- and *a*(*b*)*c*-planes by using a Nanoindenter XP™ device and a diamond Berkovich stylus. The instrumented indentation technique is the suitable method to study the tribo-mechanical behavior of such single crystals, due to its lowest dimensions. The scratching loads were applied in two different conditions: (i) 50 mN under constant loading; and (ii) ramping load up to 100 mN. The scratch was 300 μm length following the indenter edge direction. The tip penetration profiles were monitored before, during and after the scratch tests, taking into account the original surface topography, using 30 μN. As a result, it was possible to observe the elastic recovering in the scratching groove. Instrumented indentation tests, using normal loading of 100 mN, were also performed with the same facility. The scratch microstructures were observed with optical and scanning electron microscopy (SEM) and atomic force microscopy (AFM).

Specifically for the AFM, a commercial AFM system (SPM-9600 Shimadzu) in non-contact mode was used. The images were processed to remove the low-frequency noise. All AFM results reported in this work were obtained with silicon cantilevers (NCHR-20 from Nano World Innovative Technologies, respectively). The probe was Al-coated on the detector side. The cantilever had a resonant frequency of approximately 320 kHz, with nominal spring constants of 42 N/m.

3. Results and discussion

Results presented in a previous study [10] showed that the melt-textured sample is highly oriented along the *c*-axis. The highly layered structure of this material affects the morphology of the scratches and will be discussed later. Regarding resistivity, the critical temperature, T_C, is around 14.5 K. The transition width, ΔT, is approximately 0.6 K. These results indicate the good crystalline quality of the samples. Further details about the characterization can be found in Ref. [10].

Fig. 1 shows SEM micrographs of nanoscratches performed in the $FeSe_{0.5}Te_{0.5}$ single crystals with constant loading at 50 mN, for the *ab*-plane and the *a*(*b*)*c*-plane. The scar features are seemingly constant through all the scratch lengths. The scar in the *ab*-plane presents displaced material both laterally around the groove and in front of the indenter, which are typically ductile material features [11]. Notwithstanding, some released debris can also be visualized in the scar neighborhood. As shown in the inset, some removed material also remained inside the track. This indicates that the material is moved together with the indenter tip, possibly by plowing. In contrast with what is observed in Fig. 1(a), in the nanoscratch of the *a*(*b*)*c*-plane, Fig. 1(b), there is no material displaced around the groove or at the end of the scratch. Inside the scratch it is possible to observe several cracks running parallel to the *c*-axis, as shown in the inset, while the scratching direction is perpendicular. Such behavior for the *a*(*b*)*c*-plane, differently from the *ab*-plane, is typically observed in brittle materials [11].

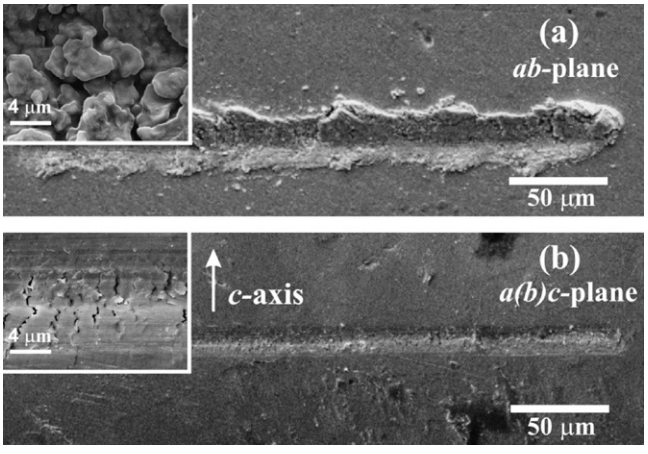

Fig. 1. SEM images of a nanoscratch under constant load of 50 mN in the (a) *ab*-plane and (b) in the *a*(*b*)*c*- plane of a $FeSe_{0.5}Te_{0.5}$ sample.

The scratch profiles obtained during and after the 50 mN constant loading, and the SEM images from the scar middle region, are shown in Fig. 2(a–d) for the *ab*- and *a*(*b*)*c*-planes, respectively. These results correspond to the tests presented in Fig. 1. In both profiles it is possible to observe the elastic recovery of the surface after load removal. In the *ab*-plane, Fig. 2(a), the material displacement at the track ending, and also the rough groove topography, are observed in the curves. In the *a*(*b*)*c*-plane, Fig. 2(c), the scratch profile is smoother than in *ab*-one, in agreement with the observations of Fig. 1(b) where material displacement is negligible. It can also be observed from the profiles that the groove is deeper in the *ab*-plane 1900 ± 760 nm than in the *a*(*b*)*c*-plane 1600 ± 300 nm, possibly indicating the *a*(*b*)*c*-plane is more wear resistant than the *ab*-plane. Another indicative of the wear resistance is the groove width, estimated from Fig. 2(b) and (d) as 20.3 ± 1.1 μm and 12.6 ± 0.5 μm, respectively. On the other hand, the averaged elastic recovery is higher in *ab*-plane (54%) than in the *a*(*b*)*c*-plane (35%).

In order to assess the materials behavior under increasing load rate, additional tests were performed using ramping load up to 100 mN. The scratch profiles during and after such regime, with the corresponding close-up SEM images for the maximum load, are shown in Fig. 3 for the (a-b) *ab*-plane and (c-d) *a*(*b*)*c*-plane. The difference between the loading and the residual profiles is due to the sample elastic recovery. The scratch under ramping load, in spite of the different work conditions, presented mostly the same basic features as in the constant load condition, Fig. 2, as follows. The profile in the *ab*-plane is rough, in agreement with the plastic deformation mechanism observed by SEM, Figs. 1(a), 2(b) and 3(b), where the material accumulates at the edges and end of the scratch. On the other hand, the profile for the *a*(*b*)*c*-plane in Fig. 3(c) is smoother, with the residual depth profile accompanying the crack-dominated groove topography. Conspicuous is the large pile-up in the *ab*-plane, Fig. 3(b), and the absence of such character in the *a*(*b*)*c*-one, Fig. 3(d). Despite the evident anisotropic behavior between *ab*- and *a*(*b*)*c*-planes, as already seen in Fig. 2, the material response under increasing tangential load persists in the analyzed load range, that is, with the dominant plastic deformation mechanism in the *ab*-plane, and the microcracking dominant mechanism in the *a*(*b*)*c*- crystallographic orientation.

Fig. 4(a) and 4(b) shows typical AFM images and profiles of scratches performed in the *ab*- and *a*(*b*)*c*-planes. Several differences are observed between them. In the *ab*-plane, there is considerable piling-up process at the scratch border meaning intensive material displacement. In the *a*(*b*)*c*-plane, it is possible to observe that the material shows several features inside the scar with crystallographic orientation parallel to the scratch direction. Also, that there is no piling-up at the groove border. These observations are in agreement with Figs. 2 and 3 where considerable accumulation of material is observed around and in the end of the scratch for the *ab*-plane but almost none for the *a*(*b*)*c*-plane.

In the search of a useful parameter to assess the $FeSe_{0.5}Te_{0.5}$ wear resistance under nanoscratch testing with a diamond tip, one could consider the wear rate, defined by the plastically displaced volume to the track length ratio [12]. However, the intense and non-regular piling-up showed by Figs. 1(a) and 2(b),